ORIGINAL ARTICLE

Pollution State Modeling for Mexico City

Philip A. White[1]* | **Alan E. Gelfand PhD**[1] | **Eliane R. Rodrigues PhD**[2] | **Guadalupe Tzintzun**[3]

[1]Department of Statistical Science, Duke University, Durham, NC, United States of America

[2]Instituto de Matemáticas, Universidad Nacional Autónoma de México, Mexico

[3]Instituto Nacional de Ecología y Cambio Climático, Secretaría de Medio Ambiente y Recursos Naturales, Mexico

Correspondence
Philip White, Department of Statistical Science, Duke University, Durham, NC, 27708, United States of America
Email: philawhite@gmail.com

Funding information
The work of Eliane Rodrigues was partially funded by the project PAPIIT-IN102416 of the Dirección General de Apoyo al Personal Académico of the Universidad Nacional Autónoma de México, Mexico (DGAPA-UNAM).

Ground-level ozone and particulate matter pollutants are associated with a variety of health issues and increased mortality. For this reason, Mexican environmental agencies regulate pollutant levels. In addition, Mexico City defines pollution emergencies using thresholds that rely on regional maxima for ozone and for particulate matter with diameter less than 10 micrometers (PM_{10}). To predict local pollution emergencies and to assess compliance to Mexican ambient air quality standards, we analyze hourly ozone and PM_{10} measurements from 24 stations across Mexico City from 2017 using a bivariate spatiotemporal model. With this model, we predict future pollutant levels using current weather conditions and recent pollutant concentrations. Employing hourly pollutant projections, we predict regional maxima needed to estimate the probability of future pollution emergencies. We discuss how predicted compliance to legislated pollution limits varies across regions within Mexico City in 2017. We find that predicted probability of pollution emergencies is limited to a few time periods. In contrast, we show that predicted exceedance of Mexican ambient air quality standards is a common, nearly daily occurrence.

KEYWORDS
Bayesian inference, environmental exposure, ozone, particulate matter, spatio-temporal modeling

* Corresponding Author

1 | INTRODUCTION

Long-term exposure to air pollution is strongly linked with respiratory and cardiovascular disease. Particulate matter (PM), and in particular those with diameter less than 10 μm (PM_{10}), is known to increase human mortality and morbidity (see, e.g., Brunekreef and Holgate, 2002; Pope III and Dockery, 2006; Loomis et al., 2013; Hoek et al., 2013). Ozone is linked to a variety of negative health outcomes, including short-term respiratory events, long-term respiratory disease, increased mortality, and low birth weight (see, e.g., Lippmann, 1989; Salam et al., 2005; Bell et al., 2006; Weschler, 2006). Because of these adverse outcomes, regulatory agencies institute policies to monitor and limit levels of these pollutants. Urban areas are often monitored more closely to protect larger populations due to higher pollution levels found in urban environments (see, e.g., Heal and Hammonds, 2014). The detrimental health effects of air pollution in the Mexico City metropolitan area, our area of interest here, are well-studied (see Mage et al., 1996; Romieu et al., 1996; Hernández-Garduño et al., 1997; Loomis et al., 1999; Bravo-Alvarez and Torres-Jardón, 2002; Barraza-Villarreal et al., 2008; Riojas-Rodríguez et al., 2014) leading to various pollution regulations in the city.

Recent standards decrease allowable pollution levels relative to previous thresholds (Diario Oficial de la Federación, 2014a,b). The ozone thresholds were reduced to 95 parts per billion (ppb) or, equivalently, 0.095 parts per million (ppm) for *hourly* ozone and 70 ppb for *eight-hour average* ozone (Diario Oficial de la Federación, 2014b). Additionally, the allowable 24-hour average PM_{10} concentration threshold was lowered to 75 micrograms per cubic meter ($\mu g/m^3$) (Diario Oficial de la Federación, 2014a).

The United States Environmental Protection Agency (EPA) limits 24-hour average PM_{10} concentration to not exceed 150 $\mu g/m^3$ and 8-hour average ozone concentration to not exceed 70 ppb. (101st United States Congress, 1990). The European Union restricts 24-hour average PM_{10} concentration to not exceed 50 $\mu g/m^3$ and 8-hour average ozone concentration to not exceed 120 ppb (European Environment Agency, 2016). Thus, by comparison, Mexican ambient air quality standards (which we denote as MAAQS) are progressive. However, declaration of pollution emergencies in Mexico City are not related to the Mexican national standards and instead use more permissive thresholds.

Mexico City's thresholds, established by the Atmospheric Environmental Contingency Program in Mexico City, are used to indicate times when pollutant concentrations are high enough to cause significant damage to human health (Administración Pública de la Ciudad de México, 2016). These goals differ from those specified for Mexico's ambient air quality standards. When emergency phases (or events) are activated, the aim is to control/decrease harmful emission levels. These thresholds have decreased over time. For instance, the thresholds for declaring the equivalent emergencies 1995-2000 were 1.5-2 times the current limits, depending on the type of emergency declared (Departamento del Distrito Federal et al., 1996).

The Mexico City metropolitan area is split into five regions: northeast (NE), northwest (NW), central (CE), southeast (SE), and southwest (SW). Within these five regions, there are 24 monitoring stations that recorded both hourly ozone and PM_{10} levels during the year 2017. Environmental alerts are declared if either hourly ozone or 24-hour average PM_{10} levels exceed certain pollutant-specific thresholds which rely on regulatory suggestions that differ from those presented in Diario Oficial de la Federación (2014a,b). Depending on the levels of the pollutant, either a phase I or a phase II alert is declared. Phase I is declared when hourly ozone exceeds $L_1^O = 0.154$ ppm (154 ppb) or 24-hour average PM_{10} exceeds $L_1^{PM} = 214\ \mu g/m^3$. Similarly, phase II is declared when hourly ozone exceeds $L_2^O = 0.204$ ppm (204 ppb) or 24-hour average PM_{10} exceeds $L_2^{PM} = 354\ \mu g/m^3$. Phase II institutes stricter protocols than phase I. See Administración Pública de la Ciudad de México (2016) for full details regarding Mexico City's pollution emergency phases.

Compared to MAAQS, Mexico City's Atmospheric Environmental Contingency Program, thresholds are more tolerant of high pollution levels. The phase I thresholds for ozone are 1.6 times the Mexican legal limits, while the phase

I thresholds for PM_{10} are almost three times the MAAQS. The phase II thresholds are roughly two and five times the MAAQS for ozone and PM_{10}, respectively. Phase alerts can be triggered both for regions and city-wide. They are driven by maxima over stations within regions, at hourly scale for ozone and 24-hour scale for PM_{10}. Explicit description is summarized in Table 1.

Phase	Region-wide Alert	City-wide Alert
None	• $PM_{10} < L_1^{PM}$ and $O_3 < L_1^O$ for all regions	• $PM_{10} < L_1^{PM}$ and $O_3 < L_1^O$ for all regions
	• No higher-order alerts supersede	
I	• $PM_{10} \geq L_1^{PM}$ within the region	• $O_3 \geq L_1^O$ for any region
	• And no higher-order alerts supersede	• Or $PM_{10} \geq L_1^{PM}$ for two or more regions
		• And no higher-order alerts supersede
II	• $PM_{10} \geq L_2^{PM}$ within the region	• $O_3 \geq L_2^O$ for any region
		• Or $PM_{20} \geq L_2^{PM}$ for two or more regions

TABLE 1 Description of Mexico City emergency phase alerts. Note that ozone thresholds are for hourly ozone, while PM_{10} limits are for 24-hour running average PM_{10}.

Pollution emergency phases are suspended only when pollution levels for every station drop below phase I thresholds (i.e. the conditions for no phase alerts are met). For practical reasons, evaluation of the emergency phases is carried out three times daily: at 10 AM, 3 PM, and 8 PM (Administración Pública de la Ciudad de México, 2016). Ultimately, however, phase activation and suspension are dependent on meteorological forecasts in addition to observed pollution levels. Because the additional meteorological criteria are not explicitly outlined, we do not attempt to predict actual phase occurrence but instead quantify the *risk* of a phase occurrence.

The contribution here is to understand and predict how often Mexico City was at risk of a pollution emergency in terms of (1) the Atmospheric Environmental Contingency Program in Mexico City and (2) current Mexican ambient air quality standards. For both, we assess how the risk of dangerous pollution varies over city regions and over time. With regard to MAAQS, we can do inference at each of three spatial scales: station-level, region-level, or city-level. Again, we may be interested in exceedances occurring on a daily scale rather than hourly. Using model choice over a selection of models, we adopt a single hierarchical bivariate spatiotemporal model for hourly ozone and PM_{10} levels. From this model, all prediction and inference regarding emergency phases and legislation-based exceedances becomes a post-model fitting exercise, as we demonstrate.

There is a rich literature on modeling PM at both coarse ($10\mu m$) and fine ($2.5\mu m$) scale as well as O_3. We note some papers relevant to our analysis. Sahu et al. (2007) use a hierarchical space-time model to model square-root ozone with the goal of assessing long term trends in ozone in Ohio. Cocchi et al. (2007) adopt a hierarchical model for log-PM_{10} concentrations to characterize the effect of meteorological conditions on the PM_{10} process and to estimate PM_{10} at unmonitored locations. Berrocal et al. (2010) model square-root ozone using spatially-varying regression coefficients (Gelfand et al., 2003) with misaligned data of two types, output from numerical models and data collected from monitoring networks. Huang et al. (2018) model log-PM_{10} and log-nitrogen dioxide (NO_2) jointly with regard to effects on health outcomes in Scotland. Similarly, we adopt a hierarchical space-time model with site-specific regression and auto-regressive coefficients for square-root ozone and log-PM_{10} concentrations in Mexico City.

In Section 2 we present exploratory data analysis for the Mexico City pollution dataset. In Section 3, we discuss modeling decisions, model fitting, inference, and selection. In Section 4 we first present a comprehensive analysis of Mexico City's phase alert system, predicting pollution levels and associated phase levels at 10 AM, 3 PM, and 8 PM to

mirror the actual phase activation and suspension procedure. Then, we carry out inference on MAAQS exceedances and compare these results to emergency phase predictions. We provide concluding discussion regarding our results and statistical modeling in Section 5.

2 | MEXICO CITY POLLUTION DATASET

We have hourly ozone and PM_{10} measurements at $N_s = 24$ stations across Mexico City, Mexico for the year 2017. Measurements are obtained minute by minute at each station and averaged to hours. Consequently, we observe measurements over $N_t = 8760$ times at each station, giving $N = 210240$ pairs of ozone and PM_{10} concentration across the 24 stations, across the entire year.[1] Relative humidity (RH) and temperature (TMP) are measured over the same space-time grid as ozone and PM_{10} and are used as explanatory variables.

As mentioned above, Mexico City is partitioned into five regions which are employed for defining environmental alert phases. Abbreviated station names, corresponding regions, and annual summaries of pollution levels are given in Table 2. Station locations are plotted in Figure 1. Besides being on the main wind path (from NE to SW) and therefore receiving many ozone precursors from the NE region, the CE region is heavily-trafficked by automobile. The SW region, located at the end of the NE-SW wind corridor, receives ozone produced along this wind path, and this ozone stays trapped in the SW region due to mountains on its southwest boundary.

Region	Stations	Station Names	Annual Average Ozone	Annual Average PM_{10}
Northeast	4	ACO, SAG, VIF, XAL	28 ppb	59 $\mu g/m^3$
Northwest	6	ATI, CAM, CUT,	27 ppb	49 $\mu g/m^3$
		FAC, TLA, TLI		
Central	4	BJU, HGM, IZT, MER	29 ppb	44 $\mu g/m^3$
Southeast	4	CHO, MPA,TAH, UIZ	36 ppb	45 $\mu g/m^3$
Southwest	6	AJM, CUA, INN	34 ppb	33 $\mu g/m^3$
		MGH, PED, SFE		

TABLE 2 Station names and regions. Average ozone and PM_{10} across regions are given.

The number of stations differs across regions and pollution levels appear to vary over the regions. The northeast region has the highest average PM_{10}, while the southeast and southwest regions have the highest average ozone. Hence, the regional maxima, used for phase alerts, are expected to have very different hourly distributions. Since the maxima are taken over a small number of stations in each region, there is no reason to attempt to consider extreme value theory here. We model at the station-level rather than at the regional level so that the distributions of the regional maxima are *induced* by the station-level modeling. In this regard, because ozone and PM_{10} are strictly non-negative, we consider either models using transformations to $\mathbb{R}^1$ or models for strictly positive data.

Region-specific box-plots for ozone and PM_{10} are shown in Figures 2a and 2b. For ozone, the SE region has the highest mean, but the CE and SW regions have the most extreme values. Note that the NE region has the highest average PM_{10}, as well as the most extreme values. This is because the NE region houses a large industrial section that generates many direct pollutants, including particulate matter. We explore dependence by computing station-

[1] Missing hourly measurements were imputed using the corresponding measurements at the nearest station within the same region. If no stations in that region recorded a measurement at that time, then the nearest station in a different region provided the missing value. This was done prior to our receiving the data for analysis.

specific Spearman's ρ[2] for all covariate-covariate, covariate-outcome, and outcome-outcome relationships. Since we employ the covariates as lag 1 predictors in our modeling below, we present these correlations with the outcomes. In addition, using a linear model with station-specific intercepts and regression coefficients for RH and TMP, we examine the relationship between residuals of ozone and PM_{10} to assess the need for a joint model for ozone and PM_{10}. We plot these site-specific correlation coefficients in Figure 2c.

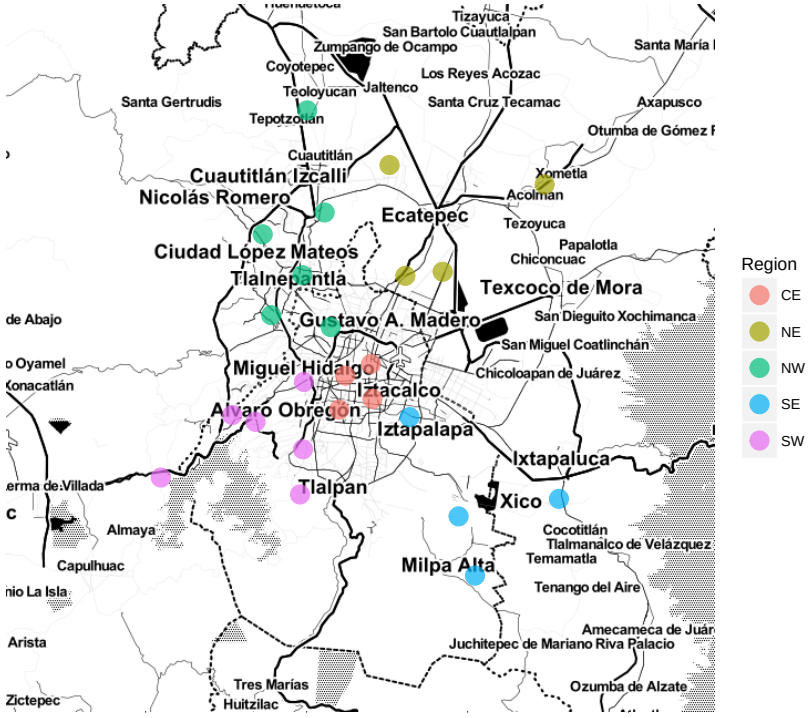

FIGURE 1 Station locations with regional labels.

The relationships between ozone and covariates (RH and TMP) are strong for all sites, while the relationships between PM_{10} and covariates (RH and TMP) vary much more across sites. However, there appears to be a strong negative correlation between RH and PM_{10} for all locations while Spearman's ρ varies greatly across sites for TMP and PM_{10}. Similarly, there is variability in the relationships between ozone and PM_{10} residuals depending on the site, motivating possible use of a joint model for ozone and PM_{10}. The variability of the outcome, covariate, and outcome-covariate relationships across stations motivates a hierarchical model for covariate effects. However, the dependence between the residuals is weak; thus, joint modeling may not offer much benefit with regard to prediction.

We find strong daily and weekly patterns for both pollutants. Using residual analysis for a model with site-specific effects for meteorological covariates, we still observe strong seasonal patterns for both day and week. Additionally, our preliminary analyses reveal strong correlation between the variance of residuals and the mean for both pollutants. This correlation could be addressed through variance stabilizing transformation (VST), e.g., log, square-root, Box-Cox as was done by, for example, Sahu et al. (2007); Cocchi et al. (2007); Berrocal et al. (2010); Huang et al. (2018).

[2] As a rank correlation, Spearman's ρ avoids concern regarding transformations and outlying values.

Alternatively, we could use heteroscedastic models that specify variance directly as a function of hour or month. We consider both approaches in Section 3.3. The associated exploratory analysis is provided in the online supplement.

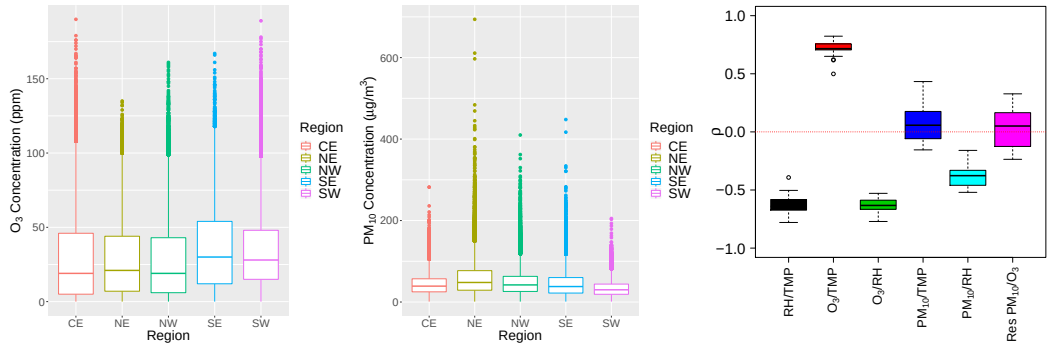

(a) Region O_3 boxplot (b) Regional PM_{10} boxplot (c) Correlation boxplots

FIGURE 2 Region-specific boxplots for (left) ozone and (center) PM_{10}. (right) Site-specific Spearman's ρ for (from left to right) relative humidity and temperature, ozone and lag-temperature, ozone and lag-relative humidity, PM_{10} and lag-temperature, PM_{10} and lag relative humidity, and model residuals for PM_{10} and ozone.

3 | METHODS AND MODELS

Given the exploratory analysis, a time-series model specification is warranted. Because the data are collected hourly, because the exposure standards are at the scale of hours (or functions of hours), and because we can identify useful discrete lags which are difficult to capture with covariance specifications, we elect to work with discrete time rather than continuous time. Additionally, our exploratory analysis suggests that a model using either a VST or time-varying variance may describe the data more accurately than models using non-transformed data or homoscedastic models. As a result, we propose the model for these data to be

$$\begin{aligned} Y_{it}^{O} &= \mathbf{x}_{i(t-1)}^{T}\boldsymbol{\beta}_{1i} + \mathbf{L}_{it}^{O\,T}\boldsymbol{\gamma}_{1i} + \psi_{1i} + \epsilon_{1it} \\ Y_{it}^{PM} &= \mathbf{x}_{i(t-1)}^{T}\boldsymbol{\beta}_{2i} + \mathbf{L}_{it}^{PM\,T}\boldsymbol{\gamma}_{2i} + \psi_{2i} + \epsilon_{2it}, \end{aligned} \tag{1}$$

where Y_{it}^{O} is ozone concentration (or square-root ozone) and Y_{it}^{PM} is PM_{10} concentration (or log-PM_{10}) at site i and hour t. Here, $\mathbf{x}_{i(t-1)}$ includes an intercept, temperature, and relative humidity at site i and time $t-1$. We use covariates from the previous hour because one of the primary purposes of this model is one-hour-ahead predictions for pollutants and corresponding phase alerts and exceedance probabilities and $\mathbf{x}_{it}$ will not be available for such prediction.

With N_s denoting the number of stations, the parameters in $\boldsymbol{\beta} = (\boldsymbol{\beta}_{11}, ..., \boldsymbol{\beta}_{1N_s}, \boldsymbol{\beta}_{21}, ..., \boldsymbol{\beta}_{2N_s})$ are station-specific regression coefficients for both PM_{10} and ozone. Because we imagine that the effect of humidity on pollutant concentrations is similar from region to region, we model regression coefficients exchangeably and hierarchically, centering effects on respective common means (see Gelman et al., 2014, for introductory thoughts on such hierarchical modeling). We define $\mathbf{L}_{it}^{O}$ and $\mathbf{L}_{it}^{PM}$ to be generic vectors of the lagged observations for ozone and PM_{10}, respectively with $\boldsymbol{\gamma} = (\boldsymbol{\gamma}_{11}, ..., \boldsymbol{\gamma}_{1N_s}, \boldsymbol{\gamma}_{21}, ..., \boldsymbol{\gamma}_{2N_s})$ as corresponding site-specific autoregressive coefficients. Lags for observations in

early January 2017 ($\mathbf{L}_{it}^{O}$ and $\mathbf{L}_{it}^{PM}$) may depend upon observations from December 2016[3]. The choice of components of $\mathbf{L}_{it}^{O}$ and $\mathbf{L}_{it}^{PM}$ becomes the model choice issue which we take up in Section 3.3. As with $\boldsymbol{\beta}$, we model $\boldsymbol{\gamma}$ hierarchically. Then, we have pure error terms, $\epsilon_{1it} \overset{iid}{\sim} N(0, \sigma_1^2)$ and $\epsilon_{2it} \overset{iid}{\sim} N(0, \sigma_2^2)$, or $\epsilon_{1it} \overset{ind}{\sim} N(0, \sigma_{1t}^2)$ and $\epsilon_{2it} \overset{ind}{\sim} N(0, \sigma_{2t}^2)$ for the heteroscedastic formulation.

Finally, to bring in spatial structure across the sites, jointly, (ψ_{1i}, ψ_{2i}) follow a bivariate conditionally autoregressive (CAR) model using coregionalization of two independent CAR models, $\mathbf{V}_1 = (V_{11}, V_{12}, ..., V_{1N_s})^T$ and $\mathbf{V}_2 = (V_{21}, V_{22}, ..., V_{2N_s})^T$ (see Rue and Held, 2005; Banerjee et al., 2014), each with precision parameter equal to 1. Explicitly,

$$\begin{pmatrix} \psi_{1i} \\ \psi_{2i} \end{pmatrix} = \mathbf{A}_\psi (V_{1i}, V_{2i})^T$$
$$\mathbf{A}_\psi = \begin{pmatrix} a_{11}^{(\psi)} & 0 \\ a_{12}^{(\psi)} & a_{22}^{(\psi)} \end{pmatrix}.$$

As a result, $\mathbf{A}_\psi$ is the Cholesky decomposition of $\mathbf{A}_\psi \mathbf{A}_\psi{}^T$ which plays the role of a site-level covariance matrix. $a_{11}^{(\psi)}$ and $a_{22}^{(\psi)}$ become positive scale parameters while $a_{12}^{(\psi)}$, the dependence parameter, can be positive or negative.

The model in (1) includes reduced models of interest. If $\alpha_{12}^{(\psi)} = 0$, then the spatial random effects are modeled as independent. Further, if $\mathbf{V}_1 = \mathbf{0}$ or $\mathbf{V}_2 = \mathbf{0}$, the model for ozone or for PM_{10} becomes non-spatial.

Because we are adopting a CAR model for point-referenced locations, we use inverse distance for the proximity matrix which we denote by $\mathbf{W}$ for $\mathbf{V}_1$ and $\mathbf{V}_2$. We assume the same distant-dependent CAR structure for both $\mathbf{V}_1$ and $\mathbf{V}_2$, with weights proportional to $\exp(-d/\max d)$ with d denoting the distance between locations and $\max d$ the maximum distance between stations.

3.1 | Priors, Model Fitting, and Prediction

We model regression and autoregressive coefficients $\boldsymbol{\beta}_{1i}, \boldsymbol{\beta}_{2i}, \boldsymbol{\gamma}_{1i}$, and $\boldsymbol{\gamma}_{2i}$ hierarchically,

$$\begin{aligned}
&\boldsymbol{\beta}_{1i} \sim N(\boldsymbol{\beta}_{01}, \Sigma_{\beta_1}), && \boldsymbol{\gamma}_{1i} \sim N(\boldsymbol{\gamma}_{01}, \Sigma_{\gamma_1}), && \Sigma_{\beta_1} \sim IW(10^3\,\mathbf{I}, p+1),\\
&\boldsymbol{\beta}_{2i} \sim N(\boldsymbol{\beta}_{02}, \Sigma_{\beta_2}), && \boldsymbol{\gamma}_{2i} \sim N(\boldsymbol{\gamma}_{02}, \Sigma_{\gamma_2}), && \Sigma_{\beta_2} \sim IW(10^3\,\mathbf{I}, p+1),\\
&\boldsymbol{\beta}_{01} \sim N(\mathbf{0}, 10^3\,\mathbf{I}), && \boldsymbol{\gamma}_{01} \sim N(\mathbf{0}, 10^3\,\mathbf{I}), && \Sigma_{\gamma_1} \sim IW(10^3\,\mathbf{I}, n_{1l}+1),\\
&\boldsymbol{\beta}_{02} \sim N(\mathbf{0}, 10^3\,\mathbf{I}), && \boldsymbol{\gamma}_{02} \sim N(\mathbf{0}, 10^3\,\mathbf{I}), && \Sigma_{\gamma_2} \sim IW(10^3\,\mathbf{I}, n_{2l}+1),
\end{aligned} \tag{2}$$

where IW denotes an inverse Wishart distribution, $p = 3$ is the number of regressors including the intercept, n_{1l} is the number of lags for ozone, and n_{2l} is the number of lags for PM_{10}. By this, we assume that station-specific regression and autoregression coefficients are exchangeable. For the variance terms in the likelihood and the CAR prior, we assume weakly informative prior distributions, where

$$\begin{aligned}
&\sigma_1^2 \sim IG(1,1), && a_{11}^{(\psi)2} \sim IG(1,1),\\
&\sigma_2^2 \sim IG(1,1), && a_{22}^{(\psi)2} \sim IG(1,1).
\end{aligned} \tag{3}$$

[3] These are available to us and are treated as fixed in our modeling.

Here, IG denotes an inverse Gamma distribution. Lastly, we assume $a_{12}^{(\psi)} \sim N(0, 10^3)$. Model fitting details via a Gibbs sampler are given in Appendices A and B.

Prediction can be done both *retrospectively*, filling in missing data over sites and times or *prospectively*, predicting the next hour given the data up to the current hour. In the latter case, we only train model parameters on data observed prior to our predictions. In fact, for computational reasons, instead of fully sequential model fitting where the model is updated hourly, we fit the model up to the last hour of the previous month. Then, this model is used to predict for pollutant levels for the upcoming month. When carrying out inference for all days simultaneously, we fit the model to all of the data. For pollution and phase predictions, we limit our prediction to 10 AM, 3 PM, and 8 PM, each day to match the times of phase activation and suspension. Even though we make one-hour-ahead predictions, our predictions depend on model parameters that are trained using all the data; thus, our phase analysis is, in a sense, retrospective even though predictions are prospective. This model allows us to make probabilistic inference about reaching the conditions for environmental phase alerts.

To predict future pollution measurements using (1), we employ posterior parameter samples in the following one-step ahead predictors:

$$\begin{aligned} Y^{O}_{i(t+1)} &= \mathbf{x}_{it}^{T}\boldsymbol{\beta}_{1i} + \mathbf{L}^{O}_{i(t+1)}{}^{T}\boldsymbol{\gamma}_{1i} + \psi_{1i} + \epsilon_{1i(t+1)} \\ Y^{PM}_{i(t+1)} &= \mathbf{x}_{it}^{T}\boldsymbol{\beta}_{2i} + \mathbf{L}^{PM}_{i(t+1)}{}^{T}\boldsymbol{\gamma}_{2i} + \psi_{2i} + \epsilon_{2i(t+1)}. \end{aligned} \tag{4}$$

In our setting, predicted phase alerts come from the one-hour-ahead ozone predictions (Y^{O*}_{it}) and the predicted 24-hour average PM_{10} concentration ($\overline{Y}^{PM*}_{it}$), where $\overline{Y}^{PM*}_{it}$ is the average of the 23 most recent observed PM_{10} concentrations ($Y^{PM}_{i(t-1)}, \ldots, Y^{PM}_{i(t-23)}$) and the forecasted PM_{10} level (Y^{PM*}_{it}). Nationally legislated thresholds depend on 24-hour average PM_{10} and on 8-hour average O_3. Similar to $\overline{Y}^{PM*}_{it}$, predicted 8-hour average ozone concentration ($\overline{Y}^{O*}_{it}$) is an average of a one-hour-ahead prediction and the previous seven ozone measurements ($Y^{O}_{i(t-1)}, \ldots, Y^{O}_{i(t-7)}$). For predictions of both $\overline{Y}^{PM*}_{it}$ and $\overline{Y}^{O*}_{it}$ in the first week of January, we use observations from late December 2016.

3.2 | Posterior Inference

The primary inferential goal is to assess how often the Mexico City metropolitan area (1) is at risk for declaring phase I or II emergencies and (2) exceeds MAAQS. To analyze the risk of phase I and II emergencies, we fit the model to all the data. In contrast, when examining pollution level exceedances, we fit the model sequentially, as described above. For both tasks, we use one-step-ahead predictions for ozone and PM_{10} concentrations.

Let j index region and d index day. Additionally, define $\overline{Y}^{PM}_{it}$ to be the 24-hour running average of PM_{10} at time t and station i and define the following maxima:

$$\begin{aligned} Z^{O}_{jt} &= \max_{i\in j} Y^{O}_{it} & W^{O}_{jd} &= \max_{t\in d}\max_{i\in j} Y^{O}_{it} \\ Z^{PM}_{jt} &= \max_{i\in j} \overline{Y}^{PM}_{it} & W^{PM}_{jd} &= \max_{t\in d}\max_{i\in j} \overline{Y}^{PM}_{it}. \end{aligned} \tag{5}$$

The Z's are regional maxima for any hour t and W's are daily regional maxima. Although these maxima rely on data observed prior to time t or day d, these quantities are used to define exceedances at time t or day d. There is limited literature about the distributions and properties of maxima for correlated random variables (see Gupta et al., 1985; Ho and Hsing, 1996). Moreover, these examples are too constrained for our application. Rather, using the definitions in (5), we do not model the maxima directly. Instead, we obtain the derived posterior predictive distributions for Z^{O}_{jt},

Z_{jt}^{PM}, W_{jd}^{O}, and W_{jd}^{PM} from posterior predictive samples of Y_{it}^{O} and Y_{it}^{PM}.

The states of Mexico City's phase alert system, $S_{jt} \in \{0, 1, 2\}$, and are completely determined by Z_{jt}^{O} and Z_{jt}^{PM} (see Section 1 and Table 1). To obtain the maximum phase alert for a day d in region j ($\max_{t \in d} S_{jt}$), we use W_{jd}^{O} and W_{jd}^{PM}. We can also infer the distribution of the highest phase alert in any region on day d ($\max_j \max_{t \in d} S_{jt}$). All these derived posteriors are obtained after model fitting. Using derived posterior predictive distributions for various maxima, as well as associated phase states and threshold exceedances, we can compute hourly and daily probabilities of (possible) phase alerts and pollution exceedances regionally and city-wide. These probabilities provide insight regarding how often the Mexico City metropolitan area is at risk of a pollution emergency.

Inference for the first task, analysis of the phase emergencies, requires analysis of regional pollution levels at 10 AM, 3 PM, and 8 PM. Specifically, phase states depend on maxima of stations over regions. If we carry out inference on a daily scale, double maxima are needed, maxima over hours and stations within regions. Because phase alerts are based upon one-hour ozone measurements and 24-hour average PM_{10}, we predict these averages as described in Section 3.1. These predictions allow us to compute predictions for derived quantities Z_{jt}^{O*}, Z_{jt}^{PM*}, W_{jd}^{O*}, and W_{jd}^{PM*}, which in turn define phase state predictions S_{jt}^{*}.

We also carry out similar inference on MAAQS exceedance for ozone and PM_{10}. Again, we are interested in regional (i.e. stations within a specified region) and city-level (i.e. at any station in the city) exceedance, hourly and daily. Again, inference for pollution exceedances relies upon maxima of one-hour ozone, eight-hour average ozone $\overline{Y}_{it}^{O}$, and 24-hour average PM_{10}. For eight-hour average ozone, we define $\overline{Z}_{jt}^{O}$ to be the regional maxima at time t and $\overline{W}_{jd}^{O}$ to be the daily maxima for region j. Because nationally legislated ozone and PM_{10} thresholds were specified to avoid reaching unsafe pollution levels, comparisons to MAAQS indicate how often Mexico City reaches such levels without triggering any city protocols. Such comparisons highlight important differences in how pollution emergencies are defined in Mexico City relative to nationally legislated levels.

3.3 | Model Selection

Here, we describe the model selection process leading to the model under which we carry out all the inference described in the previous subsections. Our model selection here centers around (1) which and how many lagged predictors are included in the model and (2) which terms of our spatiotemporal model are used, addressing whether ozone and PM_{10} random effects should be modeled jointly or whether they should be included in the model. In our exploratory analyses, we argued that the variance of ozone and PM_{10} vary with the time of day and time of year. We indicated that this could be remedied in one of two ways: using variance-stabilizing transformations to address correlation between mean and variance in the data or modeling the heteroscedasticity directly. For transformation approaches, we consider modeling the data on different scales (truncated, log, and square root) to stabilize the mean-variance correlation. To answer these modeling questions, we hold out 10% of both pollutants and treat these as missing data. Specifically, the locations and times of the hold-out data are selected at random, and both ozone and PM_{10} are held-out at these location-time pairs so that model comparison can be made using joint predictions.

We make predictions at these held-out observations and compare competing models based on the following criteria: predictive mean squared error $(E(Y_i|\mathbf{Y}_{obs}) - y_i)^2$ (PMSE) or mean absolute error $|E(Y_i|\mathbf{Y}_{obs}) - y_i|$ (PMAE), $100 \times \alpha$ % empirical coverage of nominal 90% predictive intervals, and continuous rank probability scores (CRPS) (Gneiting and Raftery, 2007), where

$$\text{CRPS}(F_i, y_i) = \int_{-\infty}^{\infty} (F_i(x) - \mathbf{1}(x \geq y_i))^2 dx = \mathbf{E}|Y_i - y_i| - \frac{1}{2}\mathbf{E}|Y_i - Y_{i'}|. \quad (6)$$

With MCMC to fit our model, we use posterior predictive samples for a Monte Carlo approximation of CRPS (see, e.g., Krüger et al., 2016),

$$\text{CRPS}(\hat{F}_i^{\text{ECDF}}, y_i) = \frac{1}{M}\sum_{j=1}^{M}|Y_j - y_i| - \frac{1}{2M^2}\sum_{j=1}^{M}\sum_{k=1}^{M}|Y_j - Y_k|, \tag{7}$$

where M is the number of MCMC samples used, Y_i are predictions, and y_i are observed values. We then average $\text{CRPS}(\hat{F}_i^{\text{ECDF}}, y_i)$ over all held-out data. For multivariate predictions, we consider the energy score (ES), which is a multivariate generalization of CRPS. For a set of multivariate predictions $\mathbf{Y}$, ES is defined as

$$\text{ES}(P, \mathbf{y}) = E_P\,\|\mathbf{Y} - \mathbf{y}\|^{\beta} - \frac{1}{2}E_P\left\|\mathbf{Y} - \mathbf{Y}'\right\|^{\beta}, \tag{8}$$

where $\mathbf{y}$ is an observation, $\beta \in (0, 2)$, and P is a probability measure (Gneiting and Raftery, 2007). It is common to fix $\beta = 1$ (see, e.g., Gneiting et al., 2008; Jordan et al., 2017). For a set of M MCMC predictions $\mathbf{Y} = \mathbf{Y}_1, ..., \mathbf{Y}_M$ for a held-out observation $\mathbf{y}$, the Monte Carlo integration for ES becomes

$$\text{ES}(\mathbf{Y}, \mathbf{y}) = \frac{1}{M}\sum_{j=1}^{M}\left\|\mathbf{Y}_j - \mathbf{y}\right\| - \frac{1}{2M^2}\sum_{i=1}^{M}\sum_{j=1}^{M}\left\|\mathbf{Y}_i - \mathbf{Y}_j\right\|. \tag{9}$$

Energy scores are scale-sensitive, meaning that if one of the variables has a much larger scale than other of the variables, it dominates the norms in (9). In our data, PM_{10} concentration in $\mu g/m^3$ takes values larger than ozone in ppb. To assure that predictions for each pollutant are similarly weighted, we standardize the predictions and hold-out values for each pollutant (i.e. subtract the sample mean and divide by the sample standard deviation). Like CRPS, we average ES over all held-out data.

The heteroscedastic models with variance that varies over hour of the day and month of the year performed uniformly worse than homoscedastic counterparts that used VST's (results not shown). Examining various combinations of square-root transformations, log transformations, and truncated distributions, we found that models using the square-root transformation for ozone and the log transformation for PM_{10} gave the best predictive performance. Turning to which and how many lagged predictors are included in the model, in Table 1 of the online supplement, we provide the results for six full models which use the square-root transformation for ozone and the log-transformation for PM_{10} but differ in terms of which lags are included. The table supports the choice of lags 1, 2, 24, and 168. Therefore, we turn to comparison of full and reduced models (with regard to (1) in Table 2 in the online supplement. The table reveals essentially no differences among the models, particularly allowing for Monte Carlo error in the values for the criteria. However, since the dependence spatial model is always preferred to the independence spatial model and since the dependence coefficient, $a_{12}^{(\phi)}$ is significantly positive, we present results for the former below.

4 | RESULTS AND DISCUSSION

We present our inference based on a joint model for ozone and PM_{10} with four lags (1, 2, 24, and 168). We use a Gibbs sampler to obtain 100,000 posterior samples after a burn-in of 10,000 iterations. Posterior parameter inference is discussed in detail in the online supplement; however, the results validate many of the modeling decisions suggested by our exploratory analysis in Section 2 and discussed in Section 3. Specifically, we infer that relative humidity negatively related to both ozone and PM_{10}. Temperature, on the other hand, is positively associated with ozone and negatively

associated with PM_{10}. The parameter $a_{12}^{(\psi)}$ is also significantly positive, indicating a positive correlation between the random effects for ozone and PM_{10}.

Turning to prediction, the predictive space is large ($2 \times N \approx 4 \times 10^5$) because we have $N = 210240$ observations. Thus, we thin the posterior predictive samples using every 10^{th} sample. By thinning, we make 10,000 roughly independent predictions. These predictions are used to carry out the analyses in Sections 4.1 and 4.2.

4.1 | Analysis of the Phase Alert System

Following Section 1, to identify when the Mexico City metropolitan area was predicted to be at risk for pollution emergencies we use one-hour-ahead predictions for pollution levels each day at: 10 AM, 3 PM, and 8 PM. Thus, our analysis predicts altogether for 1095 hours in 2017. As discussed above, we use parameter values trained on the entire dataset which enables effective prediction in early months. Because the pollutant thresholds for triggering phase alerts are very high, most of the year has very low probabilities for phase activation. However, in May of 2017 Mexico City was featured prominently in the news for having dangerously high ozone levels which led to an activation of a phase I pollution emergency. Phase probabilities aggregated over regions ($P(\max_j S_{jd} = k)$ for state k) are displayed in Figure 3. Regional phase I probabilities for each day ($P(S_{jd} = k)$ for phase k) are given in Figure 4. In Figure 4, we do not show phase II probabilities because they are so low. Additionally, we only display region NE compared to other regions because all other regions overlap (See Figure 4). Both plots (Figures 3 and 4) show high probabilities ($> 1/2$) of phase I activation from May 16th to May 25, coinciding with the time of the actually declared phase I emergency. Because this phase I alert was triggered by ozone levels, the emergency was declared city-wide, as indicated by the agreement of regional curves in Figure 4.

On April 6th, predicted ozone levels were sufficiently high to trigger a phase I emergency city-wide, although a phase alert was not declared. On only two occasions, one in January and one in December, was any region at risk of activating the emergency contingency plan due to PM_{10} levels. These high phase I probabilities were limited to the northeast region (See the red peaks in Figure 4). Again, a phase I alert triggered by PM_{10} corresponds to PM_{10} levels that are nearly three times the levels specified as safe by Mexican legislation.

In Table 3, we provide posterior means and 95% credible intervals for the number of hours and days for which the Mexico City metropolitan area is at risk for pollution emergencies ($\sum_d \mathbf{1}(S_{jd} = k)$ for phase k). There are very few hours and days when the metropolitan area or its sub-regions are at risk of pollution emergencies. That is, the posterior predictive mean for risk of a pollution emergency are, respectively, 11 days and 11 hours for the central, northwest, southeast, and southwest regions. These counts are not necessarily reflective of conditions in the central and northwest regions. Instead, these counts are indicative of predicted city-wide phase I alerts due to predicted ozone exceedances in the southeast and southwest regions, one in April and 10 in May (see Figures 3 and 4). The northeast region is the only region that had more average predicted hours and days of pollution emergency than the other regions. We predict six hours of risk for phase I emergencies in the northeast region due to PM_{10} levels over two non-consecutive days, one day in January and one in December. Because the northeast region was the only region where a predicted phase alert was triggered by PM_{10}, the predicted risk of a phase alert was limited to the northeast region. No phase alert was declared even though predicted phase probabilities were equal to one. Thus, the reason for not declaring an emergency must be attributed to meteorological conditions.

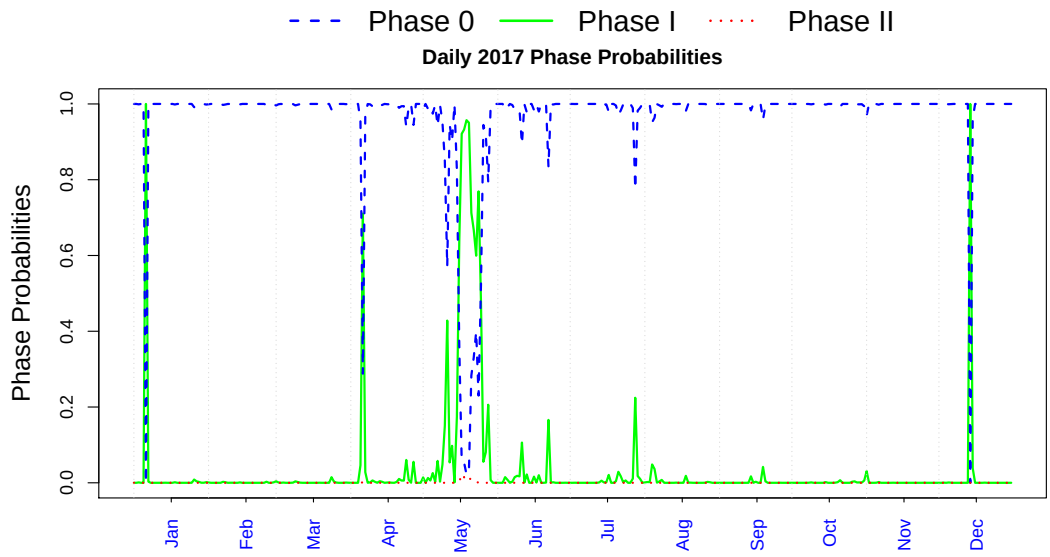

FIGURE 3 Phase probabilities in Mexico City, aggregated over all regions.

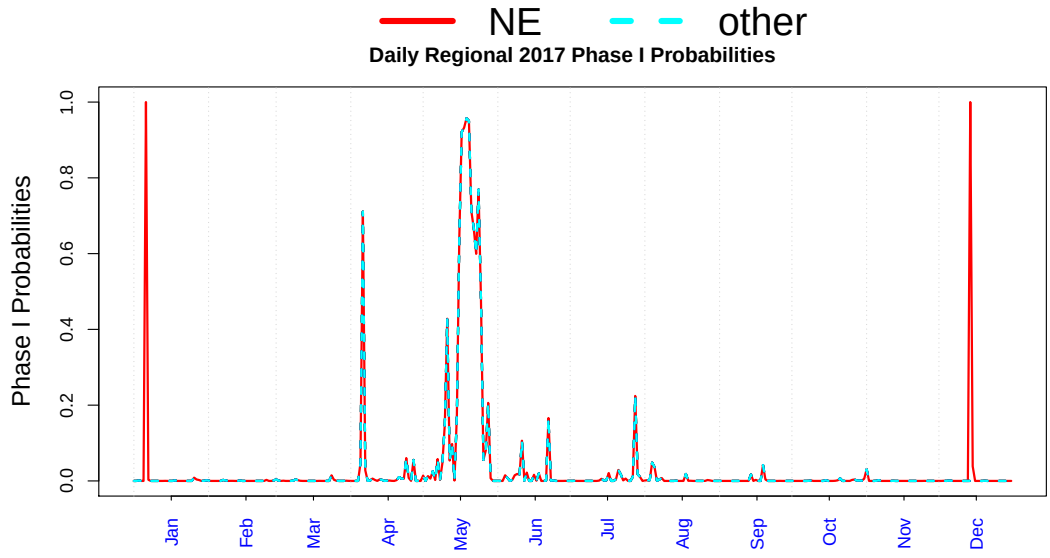

FIGURE 4 Daily phase I probabilities for Mexico City over the year by region. Phase II probabilities are not included because they are uniformly low.

	Hours (total of 1095 || 3 hours / day)					
	CE	NE	NW	SE	SW	Any
No Phase	1084 ± 4	1078 ± 4	1084 ± 4	1084 ± 4	1084 ± 4	1078 ± 4
Phase I	11 ± 4	17 ± 4	11 ± 4	11 ± 4	11 ± 4	17 ± 4
Phase II	0.09 (0,1)	0.09 (0,1)	0.09 (0,1)	0.09 (0,1)	0.09 (0,1)	0.09 (0,1)
	Days (total of 365)					
No Phase	354 ± 4	352 ± 4	354 ± 4	354 ± 4	354 ± 4	352 ± 4
Phase I	11 ± 4	13 ± 4	11 ± 4	11 ± 4	11 ± 4	13 ± 4
Phase II	0.09 (0,1)	0.09 (0,1)	0.09 (0,1)	0.09 (0,1)	0.09 (0,1)	0.09 (0,1)

TABLE 3 One-hour-ahead posterior predictive estimates for the (Top) Number of hours in each phase state for each region (Bottom) Number of days for which that phase state was attained (the maxima attained each day). Posterior means and 95% credible intervals are given for each region, using ± or parentheses. The "Any" label indicates that this is the maximum across regions.

4.2 | Comparison of Mexico City to Mexican Legislated Thresholds

Next, we examine the probability that maxima within regions exceed MAAQS on a given day (W_{jd}^{O} and W_{jd}^{PM} from Section 3.2). In contrast to phase alert probabilities, which are generally very low, exceedance probabilities are often high throughout much of the year. Because MAAQS are more reflective of healthy levels of ozone and PM_{10}, comparison between the exceedance probabilities and emergency phase probabilities highlights how often Mexico City has harmful pollution levels without triggering phase alerts. Additionally, this analysis gives insight into the probability of triggering phase alerts in Mexico City if MAAQS were adopted for Mexico City's Atmospheric Environmental Contingency Program. For our purposes, we group either type of ozone exceedance, one or eight-hour, together. In the online supplement, we focus on three months, April, August, and December, to illustrate how exceedance probabilities change over the course of the year.

We continue the prospective analysis for all months except January, fitting the model up until the last hour of the previous month to predict pollution exceedance for the month of interest[4]. Using these predictions, we give posterior means and 95% credible intervals for the one-hour-ahead predicted proportion of hours and days of exceedance for each region (i.e. $P(Z_{jt}^{O} > 95 \text{ ppb} \cup \overline{Z}_{jt}^{O} > 70 \text{ ppb})$, $P(Z_{jt}^{PM} > 75\,\mu g/m^3)$, $P(W_{jd}^{O} > 95 \text{ ppb} \cup \overline{W}_{jd}^{O} > 70 \text{ ppb})$, and $P(W_{jd}^{PM} > 75\,\mu g/m^3)$, as defined in Section 3.2). The results for ozone are given in Table 4, for PM_{10} in Table 5. For ozone, the proportion of exceedances in both hours and days decreases as latitude increases, with northern regions showing nearly half as many exceedances as the southern regions, on average. The trend for PM_{10} is less clear, although there is significant variability across regions. The northeast region has many more predicted PM_{10} exceedances than any other region. This is due to the large industrial economy located within this region. By contrast, the southwest region has very few PM_{10} exceedances.

[4] We note that prospective predictions for January will be poor because the model has not been trained on data for these times.

Ozone	Hours (total of 8016)						Days (total of 334)					
	CE	NE	NW	SE	SW	Any	CE	NE	NW	SE	SW	Any
Mean	0.147	0.066	0.093	0.194	0.186	0.252	0.651	0.367	0.499	0.671	0.696	0.794
2.5%	0.143	0.064	0.090	0.190	0.183	0.249	0.626	0.338	0.467	0.647	0.674	0.773
97.5%	0.150	0.069	0.096	0.197	0.189	0.256	0.677	0.395	0.530	0.698	0.719	0.814

TABLE 4 One-hour-ahead posterior predictive estimates for the (Left) Proportion of hours where either of the Mexican legislated ozone limits (one-hour or eight-hour) were exceeded (Right) Proportion of days where either of the Mexican legislated ozone limits were exceeded. Posterior means and 95% credible intervals are given for each region. The "Any" label indicates that at least one region has an exceedance for one or more location for the time level (hour or day).

PM_{10}	Hours (total of 8016)						Days (total of 334)					
	CE	NE	NW	SE	SW	Any	CE	NE	NW	SE	SW	Any
Mean	0.123	0.408	0.221	0.247	0.0112	0.429	0.218	0.5223	0.333	0.370	0.026	0.535
2.5%	0.122	0.406	0.219	0.245	0.0106	0.427	0.210	0.512	0.323	0.362	0.021	0.524
97.5%	0.125	0.410	0.223	0.249	0.0119	0.430	0.228	0.533	0.341	0.377	0.030	0.545

TABLE 5 One-hour-ahead posterior predictive estimates for the (Left) Proportion of hours where the Mexican legislated 24-hour PM_{10} limits were exceeded (Right) Proportion of days where either of the Mexican legislated PM_{10} limits were exceeded. The "Any" label indicates that at least one region has an exceedance for one or more location for the time level (hour or day).

Lastly, we consider the proportion of predicted hourly exceedances as a function of the month of the year and of the hour of the day. The summaries for ozone by month and hour-of-day are plotted in Figure 5, while we display PM_{10} exceedances only by month (Figure 5b). We do not plot PM_{10} exceedances as function of the hour of the day because PM_{10} exceedances depend on 24-hour averages. As a function of month, the patterns of ozone and PM_{10} exceedances are clear. For ozone, the proportion of exceedances reaches a peak in May and is high in March, April, and June. We attribute these high ozone levels to warm times of the year that are dry compared to the rainy season (June-August). PM_{10} exceedance appears to co-vary strongly with the rainy season as well, which is captured by relative humidity in our model. In particular, June, July, August, and September have almost no exceedances for PM_{10}. The coldest months (December and February) have higher probabilities of PM_{10} exceedance than warmer months that are similarly dry. Mexico City's pollution output is higher during winter festivities like Our Lady of Guadalupe, Christmas, and New Year due to fireworks and increased motor traffic. In conjunction with increased pollution output, pollution exceedances in cold months are also due to thermal inversion that traps pollution in the Valley of Mexico where Mexico City lies. Ozone exceedances also tend to peak in the afternoon to evening. Because ozone levels can exceed thresholds for either one-hour or eight-hour average ozone, we expect two peaks in ozone exceedance as a function of hour. The one-hour peak occurs around 4 PM (16:00) when the temperature is highest. The peak of eight-hour average ozone occurs around 7 or 8 PM (19:00 or 20:00), after eight hours of relatively high ozone levels. These peaks can be seen in Figure 5c.

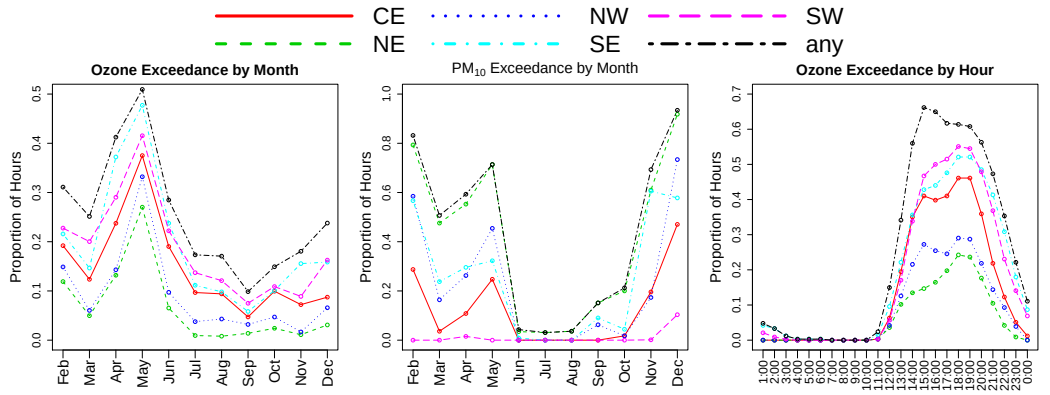

(a) O_3 exceedance by month (b) PM_{10} exceedance by month (c) Time of day O_3 exceeded

FIGURE 5 Posterior predictive means for the proportion of hours of exceedance as function of month and hour of the day.

5 | CONCLUSIONS AND FUTURE WORK

We have discussed the monitoring network for ozone and PM_{10} within Mexico City and proposed a joint spatiotemporal model for ozone and PM_{10} concentrations. This model was used to predict future pollutant concentrations. Our predictions were then used to obtain derived distributions for regional maxima of ozone and PM_{10} which are needed to determine Mexico City's pollution emergency phases. Additionally, our predictions are used to assess compliance with MAAQS. We find that predicted risk of pollution emergency is rare and are predicted for only a few periods of 2017. By contrast, we demonstrate that predicted exceedance of Mexico's ambient air quality standards is common.

In future work, we will attempt to operationalize our model so that it can be used in practice. This would require real time (hourly) fitting of the model as new measurements are available. Our modeling is amenable to sequential updating as well as possible parallelization though considerable optimization remains before this could be implemented in practice. Once implemented, our model could warn of potential pollution emergencies or compliance issues, allowing regional and city-wide adjustments, warnings, responses, and decision-making to be made earlier. Our model could also incorporate weather information to perhaps more accurately forecast pollutant levels farther ahead than our one-hour-ahead predictions.

references

101st United States Congress (1990) Clean Air Act Amendments of 1990. Public Law 101-549. 104 Stat. 2399.

Administración Pública de la Ciudad de México (2016) Órgano de difusión del gobierno de la ciudad de méxico.

Banerjee, S., Carlin, B. P. and Gelfand, A. E. (2014) *Hierarchical modeling and analysis for spatial data*. CRC Press.

Barraza-Villarreal, A., Sunyer, J., Hernandez-Cadena, L., Escamilla-Nuñez, M. C., Sienra-Monge, J. J., Ramírez-Aguilar, M., Cortez-Lugo, M., Holguin, F., Diaz-Sánchez, D. and Olin, A. C. (2008) Air pollution, airway inflammation, and lung function in a cohort study of mexico city schoolchildren. *Environmental health perspectives*, **116**, 832.

Bell, M. L., Peng, R. D. and Dominici, F. (2006) The exposure–response curve for ozone and risk of mortality and the adequacy of current ozone regulations. *Environmental health perspectives*, **114**, 532.

Berrocal, V. J., Gelfand, A. E. and Holland, D. M. (2010) A spatio-temporal downscaler for output from numerical models. *Journal of agricultural, biological, and environmental statistics*, **15**, 176–197.

Bravo-Alvarez, H. and Torres-Jardón, R. (2002) Air pollution levels and trends in the mexico city metropolitan area. In *Urban Air Pollution and Forests*, 121–159. Springer.

Brunekreef, B. and Holgate, S. T. (2002) Air pollution and health. *The lancet*, **360**, 1233–1242.

Cocchi, D., Greco, F. and Trivisano, C. (2007) Hierarchical space-time modelling of pm10 pollution. *Atmospheric environment*, **41**, 532–542.

Departamento del Distrito Federal, Gobierno del Estado de México, Secretaría de Recursos Naturales y Pesca and Secretaría de Salud (1996) Programa para mejorar la calidad del aire en el valle de mexico 1995-2000.

Diario Oficial de la Federación (2014a) Norma Oficial Mexicana NOM-020-SSA1-2014.

— (2014b) Norma Oficial Mexicana NOM-025-SSA1-2014.

European Environment Agency (2016) Exceedance of air quality limit values in urban areas.

Gelfand, A. E., Kim, H.-J., Sirmans, C. and Banerjee, S. (2003) Spatial modeling with spatially varying coefficient processes. *Journal of the American Statistical Association*, **98**, 387–396.

Gelman, A., Carlin, J. B., Stern, H. S., Dunson, D. B., Vehtari, A. and Rubin, D. B. (2014) *Bayesian data analysis*, vol. 2. CRC press Boca Raton, FL.

Gneiting, T. and Raftery, A. E. (2007) Strictly proper scoring rules, prediction, and estimation. *Journal of the American Statistical Association*, **102**, 359–378.

Gneiting, T., Stanberry, L. I., Grimit, E. P., Held, L. and Johnson, N. A. (2008) Assessing probabilistic forecasts of multivariate quantities, with an application to ensemble predictions of surface winds. *Test*, **17**, 211.

Gupta, S. S., Panchapakesan, S. and Sohn, J. K. (1985) On the distribution of the studentized maximum of equally correlated normal random variables. *Communications in Statistics-Simulation and Computation*, **14**, 103–135.

Heal, M. R. and Hammonds, M. D. (2014) Insights into the composition and sources of rural, urban and roadside carbonaceous pm10. *Environmental science & technology*, **48**, 8995–9003.

Hernández-Garduño, E., Pérez-Neria, J., Paccagnella, A. M., Piña-García, M. A., Munguía-Castro, M., Catalán-Vázquez, M. and Rojas-Ramos, M. (1997) Air pollution and respiratory health in mexico city. *Journal of occupational and environmental medicine*, **39**, 299–307.

Ho, H.-C. and Hsing, T. (1996) On the asymptotic joint distribution of the sum and maximum of stationary normal random variables. *Journal of applied probability*, **33**, 138–145.

Hoek, G., Krishnan, R. M., Beelen, R., Peters, A., Ostro, B., Brunekreef, B. and Kaufman, J. D. (2013) Long-term air pollution exposure and cardio-respiratory mortality: a review. *Environmental Health*, **12**, 43.

Huang, G., Lee, D. and Scott, E. M. (2018) Multivariate space-time modelling of multiple air pollutants and their health effects accounting for exposure uncertainty. *Statistics in medicine*, **37**, 1134–1148.

Jordan, A., Krüger, F. and Lerch, S. (2017) Evaluating probabilistic forecasts with the r package scoringrules. *arXiv preprint arXiv:1709.04743*.

Krüger, F., Lerch, S., Thorarinsdottir, T. L. and Gneiting, T. (2016) Probabilistic forecasting and comparative model assessment based on markov chain monte carlo output. *arXiv preprint arXiv:1608.06802*.

Lippmann, M. (1989) Health effects of ozone a critical review. *Japca*, **39**, 672–695.

Loomis, D., Castillejos, M., Gold, D. R., McDonnell, W. and Borja-Aburto, V. H. (1999) Air pollution and infant mortality in mexico city. *Epidemiology*, 118–123.

Loomis, D., Grosse, Y., Lauby-Secretan, B., El Ghissassi, F., Bouvard, V., Benbrahim-Tallaa, L., Guha, N., Baan, R., Mattock, H. and Straif, K. (2013) The carcinogenicity of outdoor air pollution. *The lancet oncology*, **14**, 1262–1263.

Mage, D., Ozolins, G., Peterson, P., Webster, A., Orthofer, R., Vandeweerd, V. and Gwynne, M. (1996) Urban air pollution in megacities of the world. *Atmospheric Environment*, **30**, 681–686.

Pope III, C. A. and Dockery, D. W. (2006) Health effects of fine particulate air pollution: lines that connect. *Journal of the air & waste management association*, **56**, 709–742.

Riojas-Rodríguez, H., Álamo-Hernández, U., Texcalac-Sangrador, J. L. and Romieu, I. (2014) Health impact assessment of decreases in pm10 and ozone concentrations in the mexico city metropolitan area: A basis for a new air quality management program. *salud pública de méxico*, **56**, 579–591.

Romieu, I., Meneses, F., Ruiz, S., Sienra, J. J., Huerta, J., White, M. C. and Etzel, R. A. (1996) Effects of air pollution on the respiratory health of asthmatic children living in mexico city. *American journal of respiratory and critical care medicine*, **154**, 300–307.

Rue, H. and Held, L. (2005) *Gaussian Markov random fields: theory and applications*. CRC press.

Sahu, S. K., Gelfand, A. E. and Holland, D. M. (2007) High-resolution space–time ozone modeling for assessing trends. *Journal of the American Statistical Association*, **102**, 1221–1234.

Salam, M. T., Millstein, J., Li, Y.-F., Lurmann, F. W., Margolis, H. G. and Gilliland, F. D. (2005) Birth outcomes and prenatal exposure to ozone, carbon monoxide, and particulate matter: results from the children's health study. *Environmental health perspectives*, **113**, 1638.

Weschler, C. J. (2006) Ozone's impact on public health: contributions from indoor exposures to ozone and products of ozone-initiated chemistry. *Environmental health perspectives*, **114**, 1489.

A | FULL CONDITIONAL DISTRIBUTIONS FOR AR MODEL

We give the full conditional distributions for the model specified in Section 3. We give some additional details here to clarify model fitting. Because $\mathbf{V}_1$ and $\mathbf{V}_2$ are independent *a priori*, the joint prior distribution for $\mathbf{V}_1$ and $\mathbf{V}_2$ is

$$[\mathbf{V}_1, \mathbf{V}_2] \propto \exp\left(-\frac{1}{2}\mathbf{V}_1^T Q \mathbf{V}_1\right) \exp\left(-\frac{1}{2}\mathbf{V}_2^T Q \mathbf{V}_2\right). \tag{10}$$

The induced joint prior distribution of $\begin{pmatrix}\boldsymbol{\psi}_1 \\ \boldsymbol{\psi}_2\end{pmatrix}$, where $\boldsymbol{\psi}_1 = (\psi_{11}, \psi_{12}, ..., \psi_{1N_s})^T$ and $\boldsymbol{\psi}_2 = (\psi_{21}, \psi_{22}, ..., \psi_{2N_s})^T$, is used for model fitting and can be represented as

$$[\boldsymbol{\psi}_1, \boldsymbol{\psi}_2 | A_\psi] = [\boldsymbol{\psi}_1 | A_\psi][\boldsymbol{\psi}_2 | \boldsymbol{\psi}_1, A_\psi]$$

$$\propto \exp\left(-\frac{1}{2a_{11}^{(\psi)2}}\boldsymbol{\psi}_1^T Q\boldsymbol{\psi}_1\right)\exp\left(-\frac{1}{2a_{22}^{(\psi)2}}\left(\boldsymbol{\psi}_2-\frac{a_{12}^{(\psi)}}{a_{11}^{(\psi)}}\boldsymbol{\psi}_1\right)^T Q\left(\boldsymbol{\psi}_2-\frac{a_{12}^{(\psi)}}{a_{11}^{(\psi)}}\boldsymbol{\psi}_1\right)\right). \tag{11}$$

For this section, let $\theta|\cdots$ indicate the full conditional distribution of θ, where θ is an arbitrary parameter. For several quantities, we combine site-specific variables. For example, let $Y_t^O = (Y_{1t}^O, ..., Y_{N_s t}^O)^T$, $Y_t^{PM} = (Y_{1t}^{PM}, ..., Y_{N_s t}^{PM})^T$, $\mathbf{X}_t = \text{blockdiag}(\mathbf{x}_{it})$ and $\boldsymbol{\beta}_k = (\boldsymbol{\beta}_{k1}, ..., \boldsymbol{\beta}_{kN_s})^T$. In addition to previous terms, we also let $\mathbf{L}_t = \text{blockdiag}(\mathbf{L}_{it})$ and $\boldsymbol{\gamma}_k = (\boldsymbol{\gamma}_{k1}, ..., \boldsymbol{\gamma}_{kN_s})^T$. The full conditional distributions for this model are provided below.

$$\begin{aligned}
\beta_{1i}|\cdots &\sim N(V^*_{\beta_{1i}} m^*_{\beta_{1i}}, V^*_{\beta_{1i}}) & \gamma_{1i}|\cdots &\sim N(V^*_{\gamma_{1i}} m^*_{\gamma_{1i}}, V^*_{\gamma_{1i}}) & \sigma_1^2|\cdots &\sim IG(a^*_{\sigma_1}, b^*_{\sigma_1})\\
\beta_{2i}|\cdots &\sim N(V^*_{\beta_{2i}} m^*_{\beta_{2i}}, V^*_{\beta_{2i}}) & \gamma_{2i}|\cdots &\sim N(V^*_{\gamma_{2i}} m^*_{\gamma_{2i}}, V^*_{\gamma_{2i}}) & \sigma_2^2|\cdots &\sim IG(a^*_{\sigma_2}, b^*_{\sigma_2})\\
\beta_{01}|\cdots &\sim N(V^*_{\beta_{01}} m^*_{\beta_{01}}, V^*_{\beta_{01}}) & \gamma_{01}|\cdots &\sim N(V^*_{\gamma_{01}} m^*_{\gamma_{01}}, V^*_{\gamma_{01}}) & \mathbf{V}_1|\cdots &\sim N(V^*_{V_1} m^*_{V_1}, V^*_{V_1})\\
\beta_{02}|\cdots &\sim N(V^*_{\beta_{02}} m^*_{\beta_{02}}, V^*_{\beta_{02}}) & \gamma_{02}|\cdots &\sim N(V^*_{\gamma_{02}} m^*_{\gamma_{02}}, V^*_{\gamma_{02}}) & \mathbf{V}_2|\cdots &\sim N(V^*_{V_2} m^*_{V_2}, V^*_{V_2})\\
\Sigma_{\beta_1}|\cdots &\sim IW(M^*_{\beta_1}, \nu^*_{\beta_1}) & \Sigma_{\gamma_1}|\cdots &\sim IW(M^*_{\gamma_1}, \nu^*_{\gamma_1}) & a_{11}^{(\psi)2}|\cdots &\sim IG(a^*_{a_1}, b^*_{a_1}),\\
\Sigma_{\beta_2}|\cdots &\sim IW(M^*_{\beta_2}, \nu^*_{\beta_2}) & \Sigma_{\gamma_2}|\cdots &\sim IW(M^*_{\gamma_2}, \nu^*_{\gamma_2}) & a_{22}^{(\psi)2}|\cdots &\sim IG(a^*_{a_2}, b^*_{a_2}),\\
& & & & a_{12}^{(\psi)}|\cdots &\sim N(V^*_{\psi} m^*_{\psi}, V^*_{\psi})
\end{aligned}$$

with

$$\begin{aligned}
a^*_{\sigma_1} &= 1 + \frac{N_s \times N_t}{2}\\
b^*_{\sigma_1} &= 1 + \frac{1}{2}\sum_{t=1}^{N_t}\sum_{i=1}^{N_s}(Y_{it}^O - \mathbf{x}_{it}^T\boldsymbol{\beta}_{1i} - \mathbf{L}_{it}^{O^T}\boldsymbol{\gamma}_{1i} - a_{11}^{(\psi)}V_{1i})^2\\
a^*_{\sigma_2} &= 1 + \frac{N_s \times N_t}{2}\\
b^*_{\sigma_2} &= 1 + \frac{1}{2}\sum_{t=1}^{N_t}\sum_{i=1}^{N_s}(Y_{it}^{PM} - \mathbf{x}_{it}^T\boldsymbol{\beta}_{2i} - \mathbf{L}_{it}^{PM^T}\boldsymbol{\gamma}_{2i} - a_{12}^{(\psi)}V_{1i} - a_{22}^{(\psi)}V_{2i})^2\\
m^*_{\beta_{1i}} &= \Sigma^{-1}_{\beta_1}\beta_{01} + \frac{1}{\sigma_1^2}\sum_{t=1}^{N_t}\mathbf{x}_{it}(Y_{it}^O - \mathbf{L}_{it}^{O^T}\boldsymbol{\gamma}_{1i} - a_{11}^{(\psi)}V_{1i})\\
V^*_{\beta_{1i}} &= \left(\Sigma^{-1}_{\beta_1} + \frac{1}{\sigma_1^2}\sum_{t=1}^{N_t}\mathbf{x}_{it}\mathbf{x}_{it}^T\right)^{-1}\\
m^*_{\beta_{2i}} &= \Sigma^{-1}_{\beta_2}\beta_{02} + \frac{1}{\sigma_2^2}\sum_{t=1}^{N_t}\mathbf{x}_{it}(Y_{it}^{PM} - \mathbf{L}_{it}^{PM^T}\boldsymbol{\gamma}_{2i} - a_{12}^{(\psi)}V_{1i} - a_{22}^{(\psi)}V_{2i})
\end{aligned}$$

$$\begin{aligned}
V^*_{\beta_{2i}} &= \left(\Sigma^{-1}_{\beta_2} + \frac{1}{\sigma_2^2}\sum_{t=1}^{N_t}\mathbf{x}_{it}\mathbf{x}_{it}^T\right)^{-1}\\
m^*_{\beta_{01}} &= \sum_{i=1}^{N_s}\Sigma^{-1}_{\beta_1}\boldsymbol{\beta}_{1i}\\
V^*_{\beta_{01}} &= \left(N_s\Sigma^{-1}_{\beta_1} + 10^{-3}\,\mathbf{I}\right)^{-1}\\
m^*_{\beta_{02}} &= \sum_{i=1}^{N_s}\Sigma^{-1}_{\beta_2}\boldsymbol{\beta}_{2i}\\
V^*_{\beta_{02}} &= \left(N_s\Sigma^{-1}_{\beta_2} + 10^{-3}\,\mathbf{I}\right)^{-1}\\
M^*_{\beta_1} &= 10^3\,\mathbf{I} + \sum_{i=1}^{N_s}(\boldsymbol{\beta}_{1i} - \boldsymbol{\beta}_{01})(\boldsymbol{\beta}_{1i} - \boldsymbol{\beta}_{01})^T
\end{aligned}$$

$$
\begin{aligned}
v^*_{\beta_1} &= N_s + p + 1 \\
M^*_{\beta_2} &= 10^3\,\mathbf{I} + \sum_{i=1}^{N_s} (\boldsymbol{\beta}_{2i} - \boldsymbol{\beta}_{02})(\boldsymbol{\beta}_{2i} - \boldsymbol{\beta}_{02})^T \\
v^*_{\beta_2} &= N_s + p + 1 \\
m^*_{\gamma_{1i}} &= \Sigma^{-1}_{\gamma_1}\boldsymbol{\gamma}_{01} + \frac{1}{\sigma_1^2}\sum_{t=1}^{N_t} \mathbf{L}^O_{it}(Y^O_{it} - \mathbf{x}^T_{it}\boldsymbol{\beta}_{1i} - a^{(\psi)}_{11}V_{1i}) \\
V^*_{\gamma_{1i}} &= \left(\Sigma^{-1}_{\gamma_1} + \frac{1}{\sigma_1^2}\sum_{t=1}^{N_t} \mathbf{L}^O_{it}\mathbf{L}^{O^T}_{it}\right)^{-1} \\
m^*_{\gamma_{2i}} &= \Sigma^{-1}_{\gamma_2}\boldsymbol{\gamma}_{02} + \frac{1}{\sigma_2^2}\sum_{t=1}^{N_t} \mathbf{L}^{PM}_{it}(Y^{PM}_{it} - \mathbf{x}^T_{it}\boldsymbol{\beta}_{2i} - a^{(\psi)}_{12}V_{1i} - a^{(\psi)}_{22}V_{2i}) \\
\Sigma^*_{\gamma_{2i}} &= \left(\Sigma^{-1}_{\gamma_2} + \frac{1}{\sigma_2^2}\sum_{t=1}^{N_t} \mathbf{L}^{PM}_{it}\mathbf{L}^{PM^T}_{it}\right)^{-1} \\
m^*_{\gamma_{01}} &= \sum_{i=1}^{N_s} \Sigma^{-1}_{\gamma_1}\boldsymbol{\gamma}_{1i} \\
V^*_{\gamma_{01}} &= \left(N_s\Sigma^{-1}_{\gamma_1} + 10^{-3}\,\mathbf{I}\right)^{-1} \\
m^*_{\gamma_{02}} &= \sum_{i=1}^{N_s} \Sigma^{-1}_{\gamma_2}\boldsymbol{\gamma}_{2i} \\
V^*_{\gamma_{02}} &= \left(N_s\Sigma^{-1}_{\gamma_2} + 10^{-3}\,\mathbf{I}\right)^{-1} \\
M^*_{\gamma_1} &= 10^3\,\mathbf{I} + \sum_{i=1}^{N_s} (\boldsymbol{\gamma}_{1i} - \boldsymbol{\gamma}_{01})(\boldsymbol{\gamma}_{1i} - \boldsymbol{\gamma}_{01})^T \\
v^*_{\gamma_1} &= N_s + n_{1l} + 1 \\
M^*_{\gamma_2} &= 10^3\,\mathbf{I} + \sum_{i=1}^{N_s} (\boldsymbol{\gamma}_{2i} - \boldsymbol{\gamma}_{02})(\boldsymbol{\gamma}_{2i} - \boldsymbol{\gamma}_{02})^T \\
v^*_{\gamma_2} &= N_s + n_{2l} + 1 \\
m^*_{V_1} &= \frac{a^{(\psi)}_{11}}{\sigma_1^2}\sum_{i=1}^{N_t}(Y^O_t - \mathbf{X}_t\boldsymbol{\beta}_1 - \mathbf{L}^O_t\boldsymbol{\gamma}_1) + \\
&\quad \frac{a^{(\psi)}_{12}}{\sigma_2^2}\sum_{i=1}^{N_t}(Y^{PM}_t - \mathbf{X}_t\boldsymbol{\beta}_2 - \mathbf{L}^{PM}_t\boldsymbol{\gamma}_2 - a^{(\psi)}_{22}\mathbf{V}_2) \\
V^*_{V_1} &= \left(Q_1 + \left[\frac{a^{(\psi)2}_{11}N_t}{\sigma_1^2} + \frac{a^{(\psi)2}_{12}N_t}{\sigma_2^2}\right]\mathbf{I}\right)^{-1} \\
m^*_{V_2} &= \frac{a^{(\psi)}_{22}}{\sigma_2^2}\sum_{i=1}^{N_t}(Y^{PM}_t - \mathbf{X}_t\boldsymbol{\beta}_2 - \mathbf{L}^{PM}_t\boldsymbol{\gamma}_2 - a^{(\psi)}_{12}\mathbf{V}_1) \\
V^*_{V_2} &= \left(Q_2 + \mathbf{I}\frac{a^{(\psi)2}_{22}N_t}{\sigma_2^2}\right)^{-1} \\
a^*_{a_1} &= 1 + N_s/2 \\
b^*_{a_1} &= 1 + \frac{1}{2}\boldsymbol{\psi}_1^T Q_1 \boldsymbol{\psi}_1 \\
a^*_{a_2} &= 1 + N_s/2 \\
b^*_{a_2} &= 1 + \frac{1}{2}\left(\boldsymbol{\psi}_2 - \frac{a^{(\psi)}_{12}}{a^{(\psi)}_{11}}\boldsymbol{\psi}_1\right)^T Q \left(\boldsymbol{\psi}_2 - \frac{a^{(\psi)}_{12}}{a^{(\psi)}_{11}}\boldsymbol{\psi}_1\right) \\
m^*_{\psi} &= \frac{1}{\sigma_2^2}\sum_{t=1}^{N_t}\sum_{i=1}^{N_s} V_{1i}(Y^{PM}_{it} - \mathbf{L}^{PM^T}_{it}\boldsymbol{\gamma}_{2i} - \mathbf{x}^T_{it}\beta_{2i} - a^{(\psi)}_{22}V_{2i})
\end{aligned}
$$

$$V^*_\psi = \left(10^{-3} + \frac{1}{\sigma^2_2}\sum_{t=1}^{N_t}\sum_{i=1}^{N_s} V^2_{1i}\right)^{-1}$$

B | FULL CONDITIONAL DISTRIBUTIONS FOR HETEROSCEDASTIC AR MODEL

We rely on some of the details presented in Appendix A for the CAR terms. We give the full conditional distributions for the heteroscedastic model specified in Section 3 where the variance is a function of the hour of the day $h(t)$. For this section, let $\theta|\cdots$ indicate the full conditional distribution of θ, where θ is an arbitrary parameter. We again combine several quantities for site-specific variables. Let $Y^O_t = (Y^O_{1t}, ..., Y^O_{N_s t})^T$, $Y^{PM}_t = (Y^{PM}_{1t}, ..., Y^{PM}_{N_s t})^T$, $\mathbf{X}_t = \text{blockdiag}(\mathbf{x}_{it})$ and $\boldsymbol{\beta}_k = (\boldsymbol{\beta}_{k1}, ..., \boldsymbol{\beta}_{kN_s})^T$. In addition to previous terms, we also let $\mathbf{L}_t = \text{blockdiag}(\mathbf{L}_{it})$ and $\boldsymbol{\gamma}_k = (\boldsymbol{\gamma}_{k1}, ..., \boldsymbol{\gamma}_{kN_s})^T$. The full conditional distributions for this model are provided below. If posterior parameters are not given below, then they are identical to those given for the homoscedastic model in Appendix A.

$$\begin{aligned}
\boldsymbol{\beta}_{1i}|\cdots &\sim N(V^*_{\beta_{1i}} m^*_{\beta_{1i}}, V^*_{\beta_{1i}}) & \boldsymbol{\gamma}_{1i}|\cdots &\sim N(V^*_{\gamma_{1i}} m^*_{\gamma_{1i}}, V^*_{\gamma_{1i}}) & \sigma^2_{1q}|\cdots &\sim IG(a^*_{\sigma_{1q}}, b^*_{\sigma_{1q}})\\
\boldsymbol{\beta}_{2i}|\cdots &\sim N(V^*_{\beta_{2i}} m^*_{\beta_{2i}}, V^*_{\beta_{2i}}) & \boldsymbol{\gamma}_{2i}|\cdots &\sim N(V^*_{\gamma_{2i}} m^*_{\gamma_{2i}}, V^*_{\gamma_{2i}}) & \sigma^2_{2q}|\cdots &\sim IG(a^*_{\sigma_{2q}}, b^*_{\sigma_{2q}})\\
\boldsymbol{\beta}_{01}|\cdots &\sim N(V^*_{\beta_{01}} m^*_{\beta_{01}}, V^*_{\beta_{01}}) & \boldsymbol{\gamma}_{01}|\cdots &\sim N(V^*_{\gamma_{01}} m^*_{\gamma_{01}}, V^*_{\gamma_{01}}) & \mathbf{V}_1|\cdots &\sim N(V^*_{V_1} m^*_{V_1}, V^*_{V_1})\\
\boldsymbol{\beta}_{02}|\cdots &\sim N(V^*_{\beta_{02}} m^*_{\beta_{02}}, V^*_{\beta_{02}}) & \boldsymbol{\gamma}_{02}|\cdots &\sim N(V^*_{\gamma_{02}} m^*_{\gamma_{02}}, V^*_{\gamma_{02}}) & \mathbf{V}_2|\cdots &\sim N(V^*_{V_2} m^*_{V_2}, V^*_{V_2})\\
\Sigma_{\beta_1}|\cdots &\sim IW(M^*_{\beta_1}, v^*_{\beta_1}) & \Sigma_{\gamma_1}|\cdots &\sim IW(M^*_{\gamma_1}, v^*_{\gamma_1}) & (a^{(\psi)}_{11})^2|\cdots &\sim IG(a^*_{a_1}, b^*_{a_1}),\\
\Sigma_{\beta_2}|\cdots &\sim IW(M^*_{\beta_2}, v^*_{\beta_2}) & \Sigma_{\gamma_2}|\cdots &\sim IW(M^*_{\gamma_2}, v^*_{\gamma_2}) & (a^{(\psi)}_{22})^2|\cdots &\sim IG(a^*_{a_2}, b^*_{a_2}),\\
& & & & a^{(\psi)}_{12}|\cdots &\sim N(V^*_\psi m^*_\psi, V^*_\psi)
\end{aligned}$$

with

$$\begin{aligned}
a^*_{\sigma_{1q}} &= 1 + \frac{N_s \times N_t}{2N_h}\\
b^*_{\sigma_{1q}} &= 1 + \frac{1}{2}\sum_{t=1}^{N_t}\sum_{i=1}^{N_s}(Y^O_{it} - \mathbf{x}^T_{it}\boldsymbol{\beta}_{1i} - \mathbf{L}^{O\,T}_{it}\boldsymbol{\gamma}_{1i} - a^{(\psi)}_{11}V_{1i})^2\mathbf{1}(h(t) = q)\\
a^*_{\sigma_{2q}} &= 1 + \frac{N_s \times N_t}{2N_h}\\
b^*_{\sigma_{2q}} &= 1 + \frac{1}{2}\sum_{t=1}^{N_t}\sum_{i=1}^{N_s}(Y^{PM}_{it} - \mathbf{x}^T_{it}\boldsymbol{\beta}_{2i} - \mathbf{L}^{PM\,T}_{it}\boldsymbol{\gamma}_{2i} - a^{(\psi)}_{12}V_{1i} - a^{(\psi)}_{22}V_{2i})^2\mathbf{1}(h(t) = q)\\
m^*_{\beta_{1i}} &= \Sigma^{-1}_{\beta_1}\beta_{01} + \sum_{t=1}^{N_t}\frac{1}{\sigma^2_{1h(t)}}\mathbf{x}_{it}(Y^O_{it} - \mathbf{L}^{O\,T}_{it}\boldsymbol{\gamma}_{1i} - a^{(\psi)}_{11}V_{1i})\\
V^*_{\beta_{1i}} &= \left(\Sigma^{-1}_{\beta_1} + \sum_{t=1}^{N_t}\frac{1}{\sigma^2_{1h(t)}}\mathbf{x}_{it}\mathbf{x}^T_{it}\right)^{-1}\\
m^*_{\beta_{2i}} &= \Sigma^{-1}_{\beta_2}\beta_{02} + \sum_{t=1}^{N_t}\frac{1}{\sigma^2_{2h(t)}}\mathbf{x}_{it}(Y^{PM}_{it} - \mathbf{L}^{PM\,T}_{it}\boldsymbol{\gamma}_{2i} - a^{(\psi)}_{12}V_{1i} - a^{(\psi)}_{22}V_{2i})
\end{aligned}$$

$$\begin{aligned}
V^*_{\beta_{2i}} &= \left(\Sigma^{-1}_{\beta_2} + \sum_{t=1}^{N_t}\frac{1}{\sigma^2_{2h(t)}}\mathbf{x}_{it}\mathbf{x}^T_{it}\right)^{-1}\\
m^*_{\gamma_{1i}} &= \Sigma^{-1}_{\gamma_1}\boldsymbol{\gamma}_{01} + \sum_{t=1}^{N_t}\frac{1}{\sigma^2_{1h(t)}}\mathbf{L}^O_{it}(Y^O_{it} - \mathbf{x}^T_{it}\boldsymbol{\beta}_{1i} - a^{(\psi)}_{11}V_{1i})
\end{aligned}$$

$$V^*_{\gamma_{1i}} = \left(\Sigma^{-1}_{\gamma_1} + \sum_{t=1}^{N_t} \frac{1}{\sigma^2_{1h(t)}} \mathbf{L}^O_{it} \mathbf{L}^{O^T}_{it}\right)^{-1}$$

$$m^*_{\gamma_{2i}} = \Sigma^{-1}_{\gamma_2} \boldsymbol{\gamma}_{02} + \sum_{t=1}^{N_t} \frac{1}{\sigma^2_{2h(t)}} \mathbf{L}^{PM}_{it} (Y^{PM}_{it} - \mathbf{x}^T_{it} \boldsymbol{\beta}_{2i} - a^{(\psi)}_{12} V_{1i} - a^{(\psi)}_{22} V_{2i})$$

$$V^*_{\gamma_{2i}} = \left(\Sigma^{-1}_{\gamma_2} + \sum_{t=1}^{N_t} \frac{1}{\sigma^2_{2h(t)}} \mathbf{L}^{PM}_{it} \mathbf{L}^{PM^T}_{it}\right)^{-1}$$

$$m^*_{V_1} = a^{(\psi)}_{11} \sum_{t=1}^{N_t} \frac{1}{\sigma^2_{1h(t)}} (Y^O_t - \mathbf{X}_t \boldsymbol{\beta}_1 - \mathbf{L}^O_t \boldsymbol{\gamma}_1) +$$
$$a^{(\psi)}_{12} \sum_{t=1}^{N_t} \frac{1}{\sigma^2_{2h(t)}} (Y^{PM}_t - \mathbf{X}_t \boldsymbol{\beta}_2 - \mathbf{L}^{PM}_t \boldsymbol{\gamma}_2 - a^{(\psi)}_{22} \mathbf{V}_2)$$

$$V^*_{V_1} = \left(Q_1 + \left[a^{(\psi)2}_{11} \frac{N_t}{N_h} \sum_{q=1}^{24} \sigma^2_{1q} + a^{(\psi)2}_{12} \frac{N_t}{N_h} \sum_{q=1}^{24} \sigma^2_{2q}\right] \mathbf{I}\right)^{-1}$$

$$m^*_{V_2} = \frac{a^{(\psi)}_{22}}{\sigma^2_2} \sum_{i=1}^{N_t} (Y^{PM}_t - \mathbf{X}_t \boldsymbol{\beta}_2 - \mathbf{L}^{PM}_t \boldsymbol{\gamma}_2 - a^{(\psi)}_{12} \mathbf{V}_1)$$

$$V^*_{V_2} = \left(Q_2 + \mathbf{I} a^{(\psi)2}_{22} \frac{N_t}{N_h} \sum_{q=1}^{24} \sigma^2_{2q}\right)^{-1}$$

$$m^*_{\psi} = \sum_{t=1}^{N_t} \frac{1}{\sigma^2_{2h(t)}} \sum_{i=1}^{N_s} V_{1i} (Y^{PM}_{it} - \mathbf{L}^{PM^T}_{it} \boldsymbol{\gamma}_{2i} - \mathbf{x}^T_{it} \beta_{2i} - a^{(\psi)}_{22} V_{2i})$$

$$V^*_{\psi} = \left(10^{-3} + \sum_{t=1}^{N_t} \frac{1}{\sigma^2_{2h(t)}} \sum_{i=1}^{N_s} V^2_{1i}\right)^{-1}$$